Available online at www.sciencedirect.com
ScienceDirect
European Journal of Mechanics B/Fluids 27 (2008) 771–784

On the regularity of some thermocapillary convection models

S. Nguyen *,[1], C. Delcarte, G. Kasperski [2]

Université Paris-Sud XI, LIMSI-CNRS, B.P. 133, 91403 Orsay Cedex, France

Received 10 June 2007; received in revised form 16 October 2007; accepted 3 January 2008

Available online 4 March 2008

Abstract

The classical model of confined thermocapillary convection is analyzed. Its vorticity singularity, independent of the contact angle, leads to infinite pressure values at contact lines, forbidding any numerical use of the Laplace equation to calculate free surface shapes. Four models are explored to overcome this difficulty: an explicit polynomial filtering, a Navier slip at the solid boundaries, an interface viscosity model and the combination of slip and interface viscosity. Regular solutions are obtained with the first and last approaches. Only the last one is based on physical considerations and, by the introduction of physical length scales, avoids infinite pressure values at the contact line.

Keywords: Thermocapillary flows; Spectral methods; Corner flows; Singularity

1. Introduction

Numerical simulations of wall-confined thermocapillary flows are usually based on a model inducing a vorticity discontinuity at the tri-junction occurring between a liquid–gas interface and solid boundaries. Such a vorticity singularity was first analytically displayed by Moffat [1] for a liquid in a wedge where one of the bounds is a solid wall to which the liquid sticks and the other is a liquid/gas interface on which a constant shear stress is applied. However, Moffatt did not mention the similarity between this configuration and the former one. This analogy was pointed out by Canright [2] who briefly discussed the singular features of the solution. The singular model leads to an infinite pressure value at the junction, but integrable in its vicinity, as mentioned by Kuhlmann [3]. He also highlighted some similarities between confined thermocapillary flows with static contact line and the moving contact line problem (see Dussan [4], Pismen [5]): in both cases the breakdown of the solution results in an undefined contact angle.

The numerical treatment of thermocapillary flows relies on the filtering of the singularity. Finite precision methods (finite differences, finite volumes, finite elements, etc.) are based on local formulations of the spatial derivatives which result in an implicit filter of characteristic length given by the extension of the mesh cell containing the singularity. In the case of spectral methods, the filter has to be applied explicitly on the boundary conditions. The filtering length

* Corresponding author.
E-mail addresses: sebastien.nguyen@polytechnique.edu (S. Nguyen), delcarte@limsi.fr (C. Delcarte), kasperski@fast.u-psud.fr (G. Kasperski).
[1] Present address: Laboratoire de Physique de la Matière Condensée, Ecole Polytechnique, 91128 Palaiseau Cedex, France.
[2] Present address: Laboratoire FAST, Bat. 502, Campus Universitaire, 91405 Orsay Cedex, France.

0997-7546/$ – see front matter
doi:10.1016/j.euromechflu.2008.01.008

scale is imposed by the choice of the filter. The influence of the filter on the flow was addressed by Kasperski and Labrosse [6], Chénier et al. [7]. The relevance of the filtering approach depends on the validity of Saint-Venant principle [8], that requires the stress field to be integrable on the bounds in the vicinity of the singularity.

In lid-driven cavity studies, an approach consists in subtracting the singular part of the solution and solving the resulting problem (Schultz et al. [9], Botella and Peyret [10], Auteri et al. [11]). To do so, one needs to know which kind of singularity appears, and to be able to quantify the singularity. The second point is easy to solve for the lid-driven cavity case where the answer stands in the imposed boundary conditions. For thermocapillary flows, the form of the singular solution is known (Eq. (13) of the paper of Zebib et al. [12]), but the term $\partial_x T$ which appears in the formula cannot be quantified, except for fluids with zero Prandtl number. This quantity is flow dependent, and cannot be analytically determined. Thus, singularity removal cannot be applied to thermocapillary convection.

Fluid dynamics being based on the continuous medium assumption, it is relevant to question the validity of singular models. A precise description of the physics should account for scales ranging from microscopic to macroscopic. It is still an open problem to determine which macroscopic model properly accounts for the influence of microscopic phenomena. To that end, our contribution addresses, for an incompressible and Newtonian flow, the effect of interfacial viscosity [13,14], and Navier slip boundary conditions [15] on the regularity of the macroscopic solution. A pseudo-spectral collocation code, adapted to account for interfacial viscosity (see Nguyen and Delcarte [16]), is used. The high accuracy of spectral methods allows us to assess the effects of very local scales on the flows, without intrinsic filtering. Their sensitivity to singularities allows to tackle them when no analytical study can be considered.

Section 2 introduces the concerned configuration, the different boundary condition models which will be considered and the numerical approach. In this section, the vorticity singularity is discussed for the classical approach. Section 3 presents the analytical and numerical results obtained for the different models. We conclude in Section 4.

2. Physical and mathematical model

We consider a 2D open-top rectangular box, depicted in Fig. 1, of length L and height H containing a Boussinesq fluid. The side walls at $x = \pm\frac{L}{2}$ are kept at constant temperatures T_c and T_f with $T_c > T_f$. The bottom wall is considered as adiabatic. The variation of surface tension due to the thermal gradient gives rise to thermocapillary motion in the fluid. The ratio between thermocapillary forces and buoyancy forces scales as L^{-2}, so that in the here considered shallow channel, for moderate temperature gradients, buoyancy effects play a minor role and will be ignored. At first order the surface tension is a linear function of the temperature: $\sigma(T) = \sigma(T_0) - \gamma(T - T_0)$ where the mean surface tension σ_0 is taken at the reference temperature $T_0 = \frac{T_c+T_f}{2}$ and the surface tension coefficient

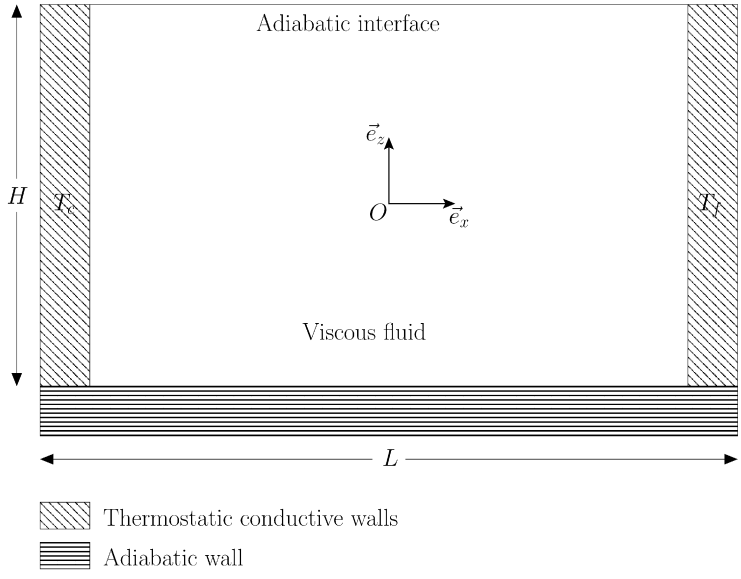

Fig. 1. Differentially heated open-boat channel.

$\gamma = -\frac{d\sigma}{dT}|_{T_0}$ is constant and commonly taken to be positive. In the limit of vanishing capillary numbers, i.e. $Ca = \frac{\gamma(T_c - T_f)}{\sigma_0} \ll 1$, the surface deformation due to the flow is negligible.

In non-dimensional form, the flow is governed by the Navier–Stokes and energy equations inside the domain $\Omega \equiv [-\frac{A_H}{2}, \frac{A_H}{2}] \times [-\frac{1}{2}, \frac{1}{2}]$, (with the aspect ratio $A_H = L/H$=2):

$$\frac{\partial u}{\partial t} + u\frac{\partial u}{\partial x} + w\frac{\partial u}{\partial z} = -\frac{\partial p}{\partial x} + Pr\,\Delta u, \tag{1}$$

$$\frac{\partial w}{\partial t} + u\frac{\partial w}{\partial x} + w\frac{\partial w}{\partial z} = -\frac{\partial p}{\partial z} + Pr\,\Delta w, \tag{2}$$

$$\frac{\partial u}{\partial x} + \frac{\partial w}{\partial z} = 0, \tag{3}$$

$$\frac{\partial \theta}{\partial t} + u\frac{\partial \theta}{\partial x} + w\frac{\partial \theta}{\partial z} = \Delta\theta. \tag{4}$$

Length, velocity, time, pressure and temperature have respectively been made dimensionless by the scales H, $u_{th} = \frac{\kappa}{H}$, $\frac{H^2}{\kappa}$, $\rho_0 u_{th}^2$ and $\theta = \frac{T - T_0}{\Delta T}$ associated to the temperature scale $\Delta T = T_c - T_f$; κ is the thermal diffusivity. The Prandtl number is defined as $Pr = \frac{\nu}{\kappa}$, where ν is the kinematic viscosity.

2.1. The classical model

In the classical model, no-slip and no-penetration conditions are imposed on the rigid walls. On the free surface, provided that the viscosity of the gas is negligible, the shear stress is balanced by thermocapillary forces. The boundary conditions are:

$$u = 0, \quad w = 0 \quad \text{at } x = \pm\frac{A_H}{2}, \tag{5}$$

$$u = 0, \quad w = 0 \quad \text{at } z = -\frac{1}{2}, \tag{6}$$

$$\frac{\partial u}{\partial z} = -Ma\,\frac{\partial \theta}{\partial x}, \quad w = 0 \quad \text{at } z = +\frac{1}{2} \text{ (Marangoni condition)}, \tag{7}$$

where $Ma = \frac{\gamma \Delta T H}{\mu\kappa}$ is the Marangoni number, μ being the dynamic viscosity.

Due to the thermal gradient on the free surface, this model presents vorticity singularities at the junctions of the free surface with the solid walls. In confined thermocapillary flows, there is always a vicinity of the junctions between the solid walls and the interface such that, in this vicinity, the flow is diffusive and the thermal field is conductive as shown in Fig. 2. The thermal gradient along the interface is thus constant and the movement is described by the problem stated by Moffatt. If one restricts to a flat interface forming an arbitrary angle with the solid wall, it can be quantitatively shown that the singularity results from the incompatibility of the boundary conditions for the velocity.

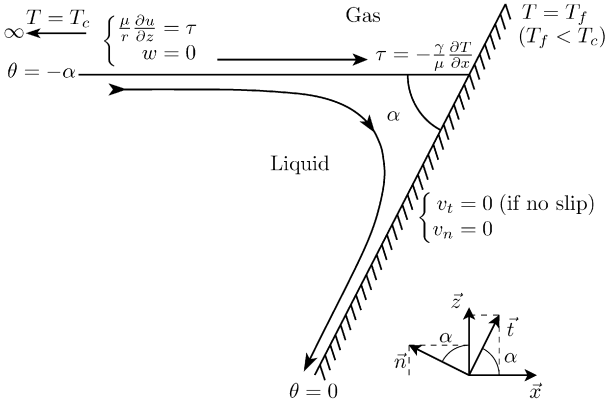

Fig. 2. The local problem of the shear stress flow.

In this analysis, we use Cartesian coordinates with the origin located at the junction, as defined in Fig. 2. The uniform Marangoni stress that applies along the interface is noted τ, regardless of its sign.

Along the solid wall, it is convenient to introduce the tangent direction, $\boldsymbol{t}$ and the normal direction, $\boldsymbol{n}$ as defined in Fig. 2: the velocity is now $v_t = \boldsymbol{V}\cdot\boldsymbol{t} = 0$ and $v_n = \boldsymbol{V}\cdot\boldsymbol{n} = 0$, with $\boldsymbol{V} = u\boldsymbol{x} + w\boldsymbol{z}$. Stating that the wall makes an angle α with the interface allows us to write: $\boldsymbol{t} = \cos\alpha\boldsymbol{x} + \sin\alpha\boldsymbol{z}$ and $\boldsymbol{n} = -\sin\alpha\boldsymbol{x} + \cos\alpha\boldsymbol{z}$, yielding: $v_t = u\cos\alpha + w\sin\alpha$ and $v_n = -u\sin\alpha + w\cos\alpha$. Noticing that, along the interface, $w = 0$ implies $\frac{\partial w}{\partial x} = 0$, and that, along the inclined wall, $v_n = 0$ (no penetration) and $v_t = 0$ (no slip), imply $\nabla v_t\cdot\boldsymbol{t} = 0$ and $\nabla v_n\cdot\boldsymbol{t} = 0$, respectively, one gets the following system of equations:

$$\frac{\partial u}{\partial z} = \frac{\tau}{\mu}, \tag{8}$$

$$\frac{\partial w}{\partial x} = 0, \tag{9}$$

$$\nabla v_n\cdot\boldsymbol{t} = -\sin\alpha\cos\alpha\frac{\partial u}{\partial x} + \cos^2\alpha\frac{\partial w}{\partial x} - \sin^2\alpha\frac{\partial u}{\partial z} + \sin\alpha\cos\alpha\frac{\partial w}{\partial z} = 0, \tag{10}$$

$$\nabla v_t\cdot\boldsymbol{t} = \cos^2\alpha\frac{\partial u}{\partial x} + \sin\alpha\cos\alpha\frac{\partial w}{\partial x} + \sin\alpha\cos\alpha\frac{\partial u}{\partial z} + \sin^2\alpha\frac{\partial w}{\partial z} = 0. \tag{11}$$

All the relations are satisfied at the junction where the boundaries meet. This system yields four unknowns which are the space derivatives of the velocity components. Taking into account (9) and the fluid incompressibility, $\frac{\partial u}{\partial x} + \frac{\partial w}{\partial z} = 0$, Eqs. (10) and (11) become:

$$\sin^2\alpha\frac{\partial u}{\partial z} = -\sin 2\alpha\frac{\partial u}{\partial x}, \tag{12}$$

$$\sin 2\alpha\frac{\partial u}{\partial z} = -2\cos 2\alpha\frac{\partial u}{\partial x}. \tag{13}$$

For any angle, excepting the limit cases, $\alpha = 0$ and $\alpha = \pi$ which are unrealistic with the hypothesis of a flat interface, the relations (12) and (13) can only be true if $\frac{\partial u}{\partial x} = \frac{\partial u}{\partial z} = 0$. This is not compatible with (8) resulting from the Marangoni stress. Beside showing quantitatively that the imposed boundary conditions are not compatible, this allows us to say that there does not exist any appropriate angle for which the singularity should disappear with the classical Marangoni stress definition and no-slip conditions. If one keeps the incompressibility of the liquid and dismisses possible non-Newtonian behaviors, the immediate implication of this discussion is to modify the boundary conditions.

2.2. Explicit polynomial filtering

In order to remove the singularity, a filter can be chosen in the set of polynomials $f_n(x) = (1 - (\frac{2x}{A_H})^{2n})^2$ so that the boundary condition (7) is replaced by:

$$\frac{\partial u}{\partial z} = -Ma\, f_n(x)\frac{\partial\theta}{\partial x}, \quad w = 0 \quad \text{at } z = +\frac{1}{2}. \tag{14}$$

A cutting length l_n can be defined as the distance from the boundaries where the regularizing function is equal to 0.9. It can be expressed as: $l_n = 1 - (1 - \sqrt{0.9})^{1/2n}$.

Assuming that the physics of the continuous medium is regular, we now introduce macroscopic models, based on more relevant physical considerations, which can incorporate local effects.

2.3. Slip boundary condition

Since the no slip condition introduces the vorticity in the solid wall boundary condition it seems relevant to try and relax it by using a Navier slip law on the solid [15]. In the configuration of Fig. 2, the tangential velocity on the inclined solid wall now obeys to:

$$b_s\nabla v_t\cdot\boldsymbol{n} = v_t$$

where b_s is the slip length. With this model, perfect slip is obtained for $b_s \to \infty$.

2.4. Interface viscosity

On the free surface it is possible to take into account dynamical modifications to the surface tension which should become important in the vicinity of the junctions. Such a model can be given by interface viscosity [13] in the formulation of Regnier et al. [17]. The stress balance along a mono dimensional interface now writes:

$$\mu \frac{\partial u}{\partial z} = \frac{\partial \sigma(T)}{\partial x} + (\varepsilon_s + \eta_s) \frac{\partial^2 u}{\partial x^2}, \tag{15}$$

where ε_s and η_s are respectively the shear and dilatational surface viscosities. These coefficients are proportional to the time required by the fluid to reorganize itself at the surface after a perturbation. A more detailed discussion can be found in Nguyen et al. [8]. The dimensionless boundary condition (7) becomes:

$$\frac{\partial u}{\partial z} = -Ma \frac{\partial \theta}{\partial x} + Vi \frac{\partial^2 u}{\partial x^2} \quad \text{at } z = +\frac{1}{2} \tag{16}$$

where $Vi = \frac{\varepsilon_s + \eta_s}{\mu H}$ is the dimensionless interface viscosity. Vila et al. in [18] analyzed experimental measurements using the theories of Bedeaux and Oppenheim [19] and of Goodrich [20]. They found an interface viscosity equal to $\sim 10^{-4}$ g s^{-1} for the mercury and then the dimensionless interface coefficient $Vi \simeq 4 \times 10^{-2}$ for a cavity of 1 cm deep.

2.5. Spectral methods

The calculation of 2D steady states is achieved using a time-stepping code. The evaluation of the space derivatives is based on a Chebyshev collocation spectral method with Gauss–Lobatto grids in both directions [21]. The time-stepping follows a usual second order backward Euler scheme with an implicit treatment of the diffusion terms. A projection–diffusion algorithm is used to uncouple the velocity and pressure fields as proposed by Batoul et al. [22] and analyzed by Leriche and Labrosse [23]. In this method, the incompressibility condition is satisfied asymptotically with the increase of the number of Chebyshev modes. The decrease of the velocity divergence is exponential for a regular solution. A singularity will limit the convergence behavior to a polynomial law, the exponent of which is related to the order and the location of the singularity [24]. The behavior of the velocity divergence will then constitute a measure of the regularity of the model. The apparent drawback of the numerical method is used to detect the presence of singularities for cases unattainable to analytical studies. For sure, for singular problems, the solutions are altered by the use of spectral methods. We wish to stress that, to our knowledge, any finite precision numerical method will alter the solution of a singular problem, by inducing some local numerical diffusion of the singularity. In the case of spectral methods, the effect is non-local.

3. Results

3.1. Polynomial filter

The left panel of Fig. 3 shows the evolution of the velocity divergence (rescaled by the maximum velocity value) with the grid refinement for several values of the filtering parameter n, the Prandtl and Marangoni numbers being respectively fixed to 1 and 1500. In the right panel, the same quantity is shown for several values of the Prandtl number and of n, the value of the Marangoni number being fixed to 1500 at $Pr \geqslant 1$ and to 500 at $Pr = 10^{-2}$ in order to get steady flows. The divergence does not decrease exponentially but following a power law aN^{-b} where N is the number of Chebyshev modes. The decreasing rate b, equal to 4, neither depends on the Prandtl and Marangoni numbers nor on the degree of the polynomial filter.

From now on, Pr and Ma will be fixed to 1 and 1500 respectively, the time-step to 10^{-4} and the grid greater than 200^2.

To set a point of comparison between the different models, we first describe and analyze the flow features of a solution obtained with a filtering polynomial of degree $n = 80$ for a number of Chebyshev modes of 320^2. This is the *best* spectral approximation to the singular problem presented in this paper. At these values the corresponding filtering length scale is $l_{80} = 1.839 \times 10^{-2}$ (see Section 2.2). The minimum and maximum horizontal mesh size, located on the

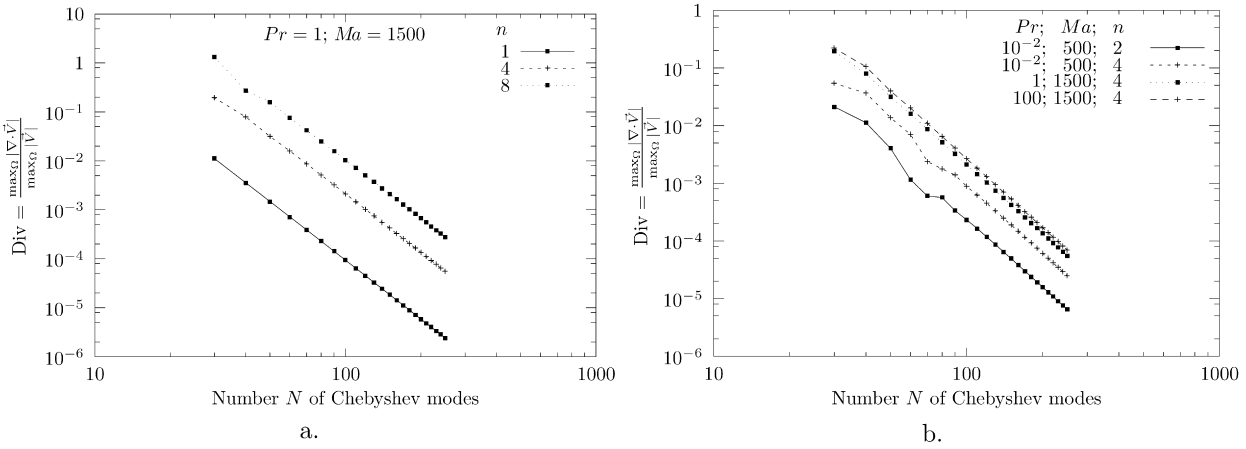

Fig. 3. Evolution of the divergence with the grid: polynomial filter.

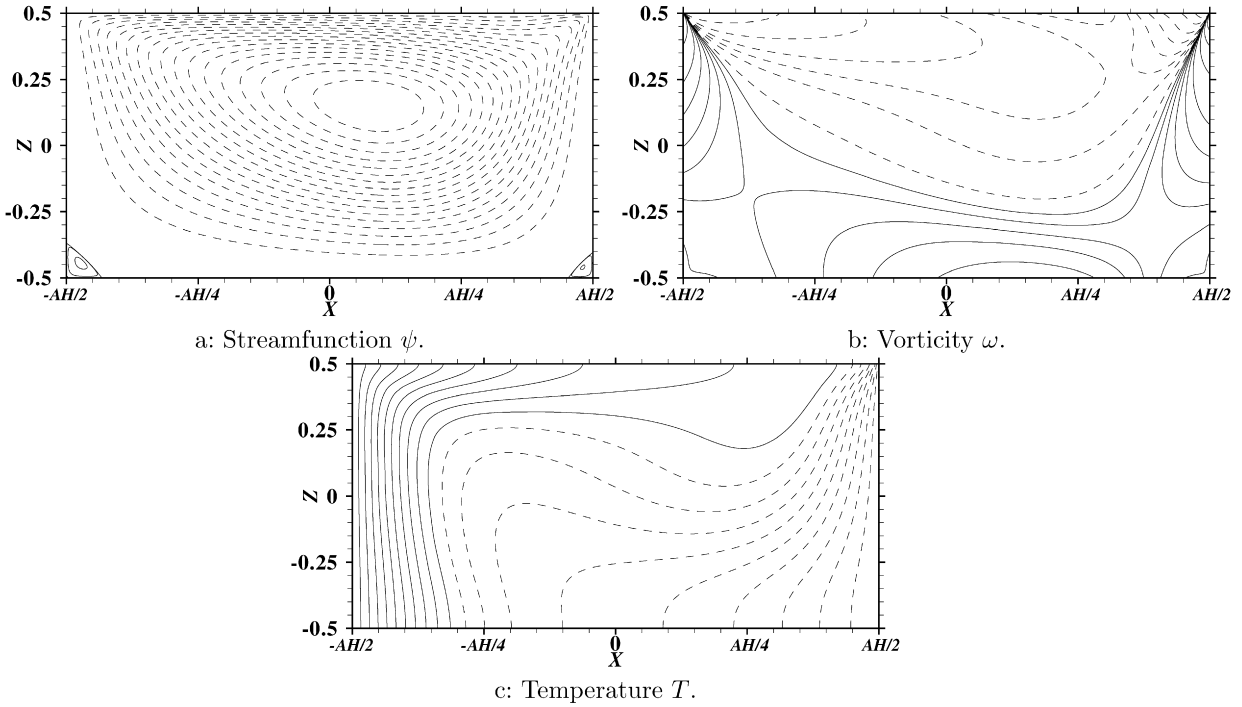

Fig. 4. Flow at $Ma = 1500$, $Pr = 1$, $n = 80$ and $N_x \times N_z = 320 \times 320$. Dashed lines correspond to negative values.

walls and around $x = 0$ respectively, are: $\Delta x_{\min} = 1 - \cos(\pi/320) = 7.710 \times 10^{-4}$ and $\Delta x_{\max} = -\cos(\pi 161/320) = 9.817 \times 10^{-3}$.

The flow structure is displayed in Fig. 4 and some profiles at the free surface in Fig. 5. The stream function exhibits a main structure, non-convex in the cold corner (top), and at least two secondary eddies in the bottom corners (Fig. 4(a)). Close to the interface, the isotherms are compressed near the cold wall (Fig. 4(c)). The thermocapillary forces are maximum in this region and the convective flow intensifies them. Therefore, the velocity profile on the free surface, displayed in the left panel of Fig. 5, is maximum near the cold wall. However, $\frac{\partial u}{\partial x}$ cancels at the top corners, as exhibited by the zooms embedded in the figure, so that the incompressibility condition is enforced. The vorticity, in Fig. 4(b), presents two zones: one of negative vorticity near the free surface where the thermocapillary stress is dominant and one of positive vorticity near the solid walls due to the viscous dissipation, the zero vorticity level going

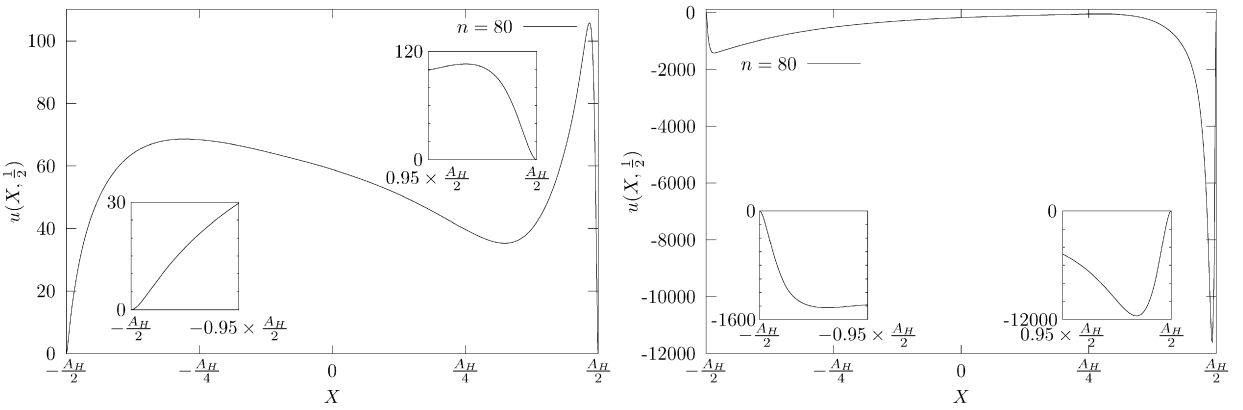

a: Horizontal component u of the velocity. b: Vorticity ω.

Fig. 5. Flow on the free surface ($Ma = 1500$, $Pr = 1$, $n = 80$ and $N_x \times N_z = 320 \times 320$).

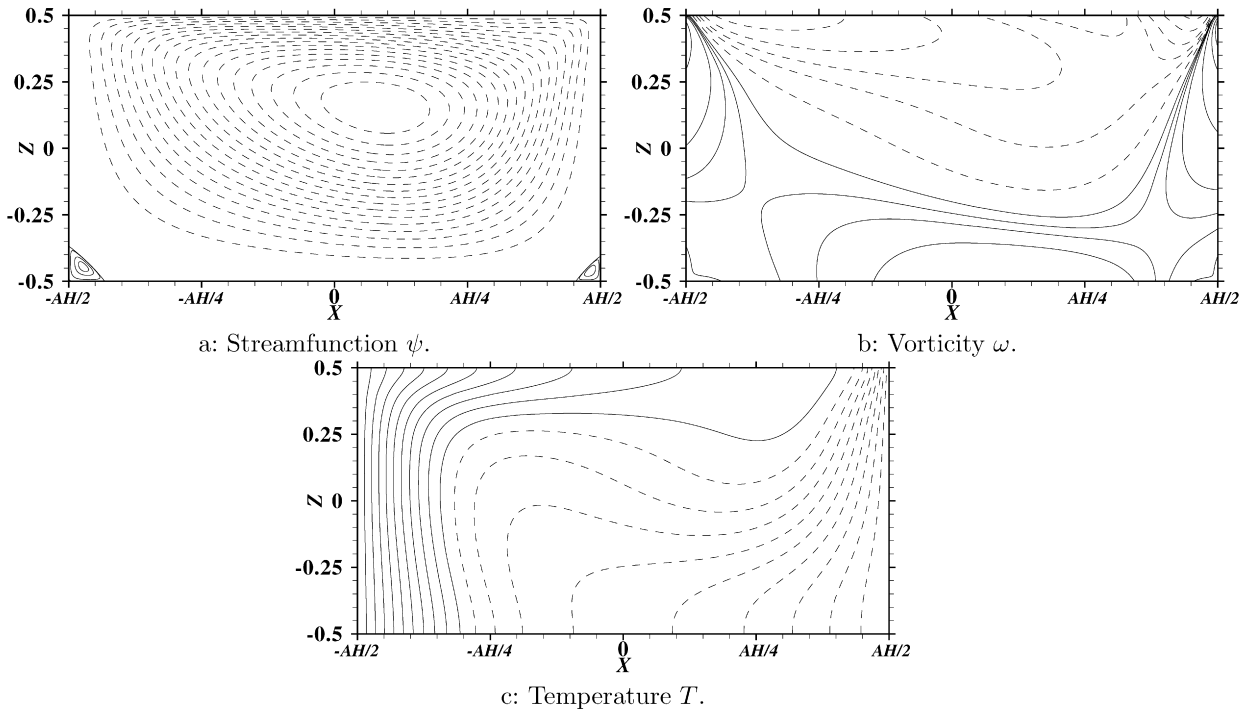

a: Streamfunction ψ. b: Vorticity ω.

c: Temperature T.

Fig. 6. Flow at $Ma = 1500$, $Pr = 1$ and $n = 4$. Dashed lines correspond to negative values.

from the warm to the cold corner. As displayed in Fig. 5(b), the vorticity gradient is much more important in the cold corner where the thermal gradient is the largest. On the free surface, velocity and vorticity present sharp extrema but both cancel at $x = \pm\frac{A_H}{2}$. This solution is very close to a solution obtained by a finite volume method with a 100×100 stretched grid ($\Delta x_{\min} \approx 2.4 \times 10^{-4}$, $\Delta x_{\max} \approx 2.3 \times 10^{-3}$) [25].

To illustrate the effect of a low degree filtering, we present the case $n = 4$. Figs. 6 and 7 show similar general features to $n = 80$. The differences with the reference solution are observed on the convexity of the stream function main eddy (Fig. 6(a)), and on the free surface profiles (Fig. 7). These last ones are the most significative of the strong filtering of the singularity. The velocity is now smaller in the cold corner than in the hot corner. This results from the dramatic decrease of the vorticity extremum in the cold corner: the $n = 4$ value is less than 10% of the $n = 80$ reference.

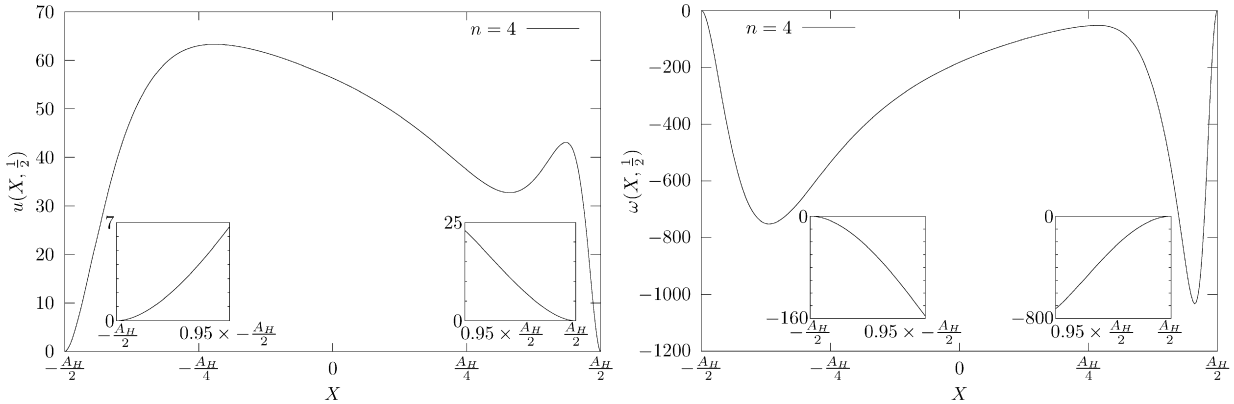

a: Horizontal component u of the velocity. b: Vorticity ω.

Fig. 7. Flow on the free surface ($Ma = 1500$, $Pr = 1$ and $n = 4$).

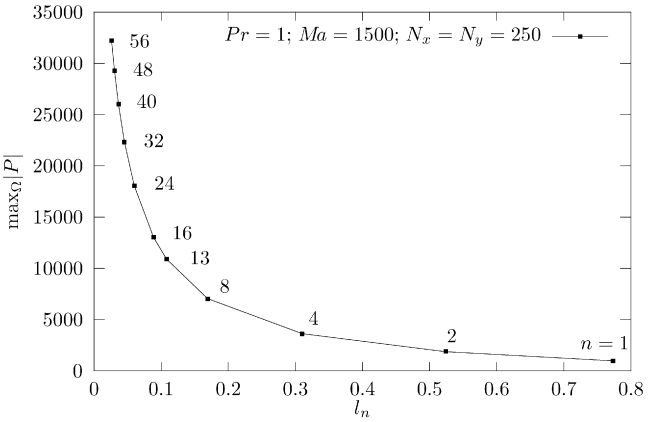

Fig. 8. Evolution of the pressure maximum with the filtering length l_n.

Table 1
Evolution with n of the pressure and divergence maxima (located in the cold corner)

n	l_n	max(P)	Div
1	0.773468	974.01979	2.39958E−06
2	0.524046	1866.1752	1.11760E−05
4	0.310106	3630.3377	5.50349E−05
8	0.169401	7039.7335	2.75620E−04
13	0.107939	10914.409	7.79838E−04
16	0.0886282	13034.662	1.16408E−03
24	0.0599945	18054.528	2.55022E−03
32	0.0453421	22331.965	4.45251E−03
40	0.0364412	26038.726	6.87415E−03
48	0.0304612	29296.331	9.80886E−03
56	0.0261671	32192.868	1.32672E−02

The choice of the filtering length scale is a major issue, it should be determined by examining the convergence of the regularized problem when l_n is decreased. When doing so, the solution is supposed to converge towards that of the unfiltered problem for which the pressure diverges logarithmically at the corners, where the singularity occurs, as shown by Kuhlmann [3]. This contradicts the convergence of the whole solution with the filter. It is also impossible to determine a relevant filtering length scale. As shown in Fig. 8 and Table 1, for a mesh of $N_x = N_z = 250$, the

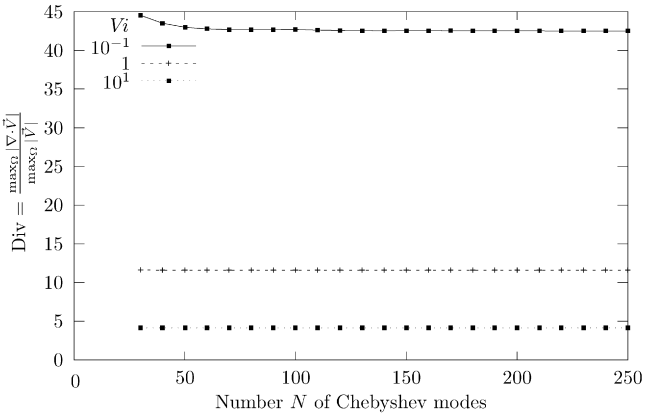

Fig. 9. Evolution of the velocity divergence with the grid refinement: interfacial viscosity model.

maximum of the pressure field diverges with l_n. This would forbid any attempt to compute a free surface shape with the Laplace equation.

Because of this issue, it is interesting to try to remove the singularity by physical considerations. This will be developed in the following sections.

3.2. Slip boundary condition

Slip boundary conditions lead to replace relation (11) by:

$$\begin{aligned}\nabla v_t \cdot \boldsymbol{n} &= -\sin\alpha\cos\alpha\frac{\partial u}{\partial x} - \sin^2\alpha\frac{\partial w}{\partial x} + \cos^2\alpha\frac{\partial u}{\partial z} + \sin\alpha\cos\alpha\frac{\partial w}{\partial z}\\ &= b_s^{-1}(u\cos\alpha + w\sin\alpha),\end{aligned} \tag{17}$$

where the second line cancels at the corner because the wall is not permeable and the junction is fixed. The same substitution as for the no slip case yields the following relations:

$$\cos^2\alpha\frac{\partial u}{\partial z} = 2\sin\alpha\cos\alpha\frac{\partial u}{\partial x}, \tag{18}$$

$$-\sin^2\alpha\frac{\partial u}{\partial z} = 2\sin\alpha\cos\alpha\frac{\partial u}{\partial x}. \tag{19}$$

For any angle different from $\alpha = 0, \pi/2, \pi$, $\frac{\partial u}{\partial z} = \frac{\partial u}{\partial x} = 0$, which yields the same incompatibility as previously with no slip conditions. When $\alpha = 0, \pi/2, \pi$, the situation is slightly different because only $\frac{\partial u}{\partial z}$ is required to vanish. This nevertheless contradicts the Marangoni stress condition $\frac{\partial u}{\partial z} = \frac{\tau}{\mu}$.

The vorticity singularity cannot be removed by a slip boundary condition whatever the imposed angle between the free surface and the solid wall. It demonstrates the physical irrelevance of the model at the junction.

3.3. Interface viscosity

No analytical analysis could be performed in this case. The efficiency of this approach to provide regular solutions is thus measured by the behavior of the velocity divergence (Fig. 9). Three values of interface viscosity have been tested: 10^{-1}, 1 and 10. The divergence tends to a non-zero constant value with the increase of the number of modes. The relative position of the curves agrees with the fact that $Vi \to \infty$ and $Vi \to 0$ respectively correspond to rigid and free surfaces.

The value $Vi = 10^{-1}$ is such that the velocity profile on the free surface is locally modified in the vicinity of strong gradients. The flow fields are quite similar to those obtained here above with the polynomial filter corresponding to $n = 4$, so they are not displayed here (they can be seen in [26]). The noteworthy difference is that $\frac{\partial u}{\partial x}$ does not cancel

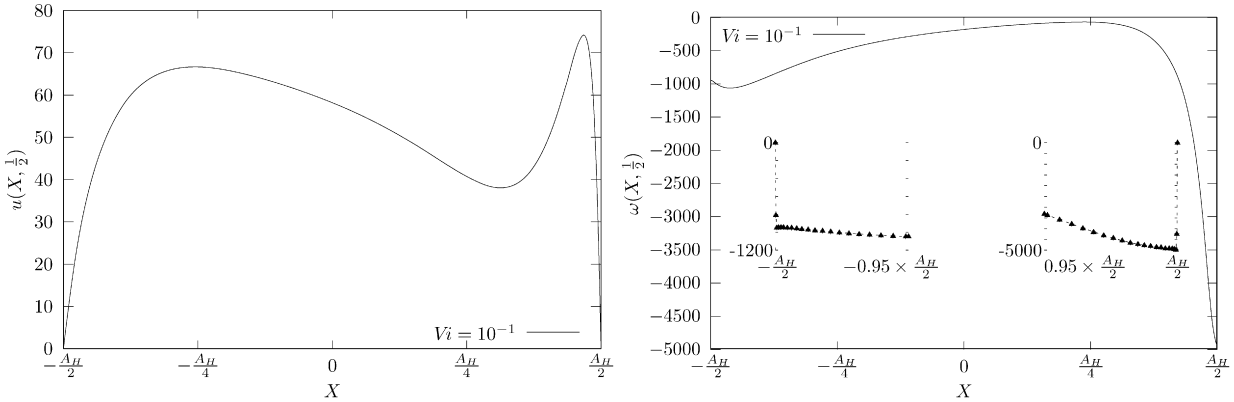

a: Horizontal component u of the velocity. b: Vorticity ω.

Fig. 10. Flow on the free surface ($Ma = 1500$, $Pr = 1$ and $Vi = 10^{-1}$).

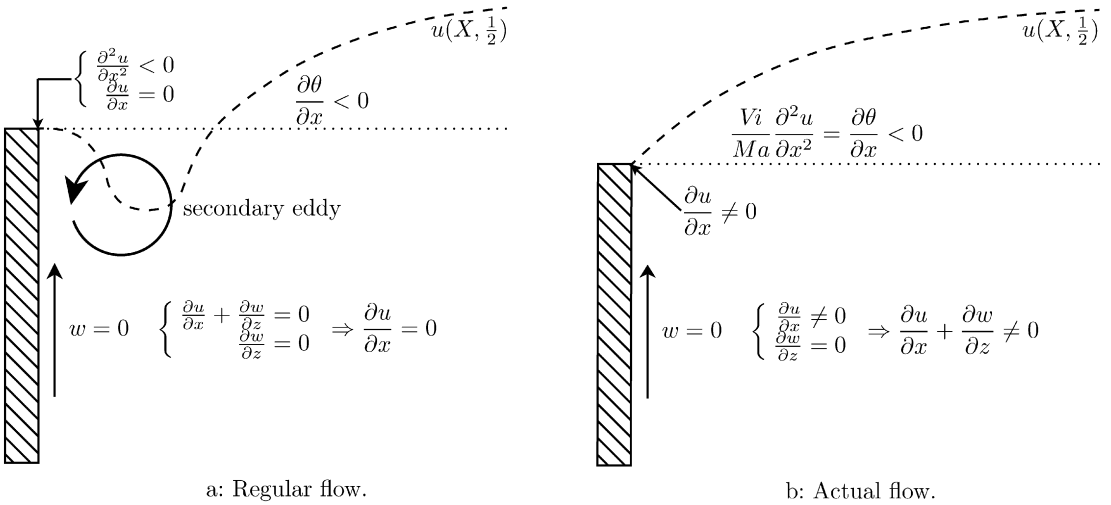

a: Regular flow. b: Actual flow.

Fig. 11. Schemes of the velocity profile at the solid/fluid junction in case of interface viscosity.

at the corners, as shown in Fig. 10(a). Fig. 7(b) reveals that the vorticity minima are near the warm and cold corners. For both of the 200^2 grid and the 250^2 grid, the cold corner minima are on the third mesh point apart from the vertical wall. This indicates that either the grid is not fine enough to capture the filter scale or the interface viscosity does not balance the thermal gradient.

Let us assume that the interface viscosity term is such that, at $x = \pm\frac{A_H}{2}$, the vorticity cancels:

$$Ma\,\frac{\partial\theta}{\partial x} = Vi\,\frac{\partial^2 u}{\partial x^2}. \tag{20}$$

Since $\frac{\partial\theta}{\partial x}$ is negative, the curvature of the velocity profile is convex. The incompressibility condition, associated with non-slip conditions on the vertical walls, leads to $\frac{\partial u}{\partial x} = 0$ at $x = \pm\frac{A_H}{2}$. As exhibited in Fig. 11(a), secondary vortices should then exist near the warm and cold corners. However, given the small values of the velocity, their origin cannot be inertial and it does not seem conceivable that the dissipative term becomes larger than the thermocapillary stress which drives the convection.

If the incompressibility of the fluid is relaxed near the top corners, the velocity profile shown in Fig. 11(b) could be obtained.

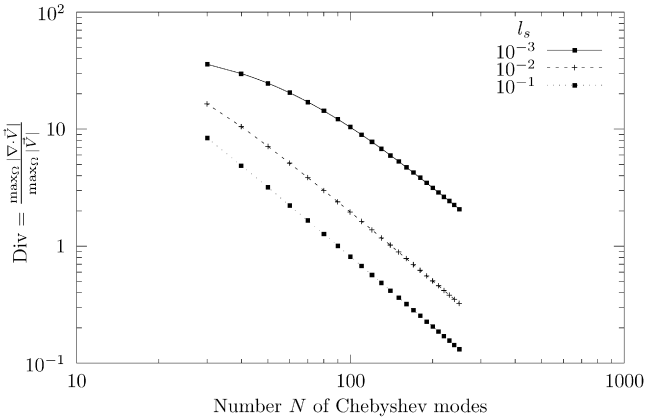

Fig. 12. Velocity divergence as a function of the grid for slip and interfacial viscosity ($Vi = 10^{-1}$).

Table 2
Coefficients of the decreasing power law of the velocity divergence; N_p is the number of points used in the fit with Mathematica

Coefficients of the power law: $\mathrm{Div}(\boldsymbol{V}) = aN^{-b}$						
Pr	*Ma*	*Vi*	l_s	a	b	N_p
1	1500	0.1	10^{-1}	$e^{9.0}$	1.99505	10
1	1500	0.1	10^{-2}	$e^{9.8}$	1.98039	7
1	1500	0.1	10^{-3}	$e^{11.0}$	1.86706	7

In conclusion, removing the vorticity discontinuity by means of a viscosity of the interface leads to non-zero values of the velocity divergence in the vicinity of the solid/fluid junctions. Nevertheless, the pressure value is defined. A Stokes local analysis gives: $\frac{\partial p}{\partial x} = \frac{\partial^2 u}{\partial x^2} = \frac{Ma}{Vi}\frac{\partial \theta}{\partial x}$.

3.4. Viscous interface and slip boundary conditions

At the surface, the boundary conditions still account for interface viscosity, but on the solid boundaries, they are now defined by:

$$u = 0, \quad \pm l_s \frac{\partial w}{\partial x} = w, \quad \text{at } x = \pm\frac{A_H}{2}, \tag{21}$$

$$\frac{\partial u}{\partial z} = -Ma\frac{\partial \theta}{\partial x} + Vi\frac{\partial^2 u}{\partial x^2}, \quad w = 0, \quad \text{at } z = +\frac{1}{2}, \tag{22}$$

$$l_s \frac{\partial u}{\partial z} = u, \quad w = 0, \quad \text{at } z = -\frac{1}{2}, \tag{23}$$

where $l_s = \frac{b_s}{H}$ is the dimensionless slip parameter. Because $\frac{\partial w}{\partial z} \neq 0$ is allowed at $x = \pm\frac{A_H}{2}$, the continuity equation can be satisfied together with $\frac{\partial u}{\partial x} \neq 0$.

The behavior of the velocity divergence with respect to the grid refinement, for three values of the slip length, is presented in Fig. 12. The interface viscosity is fixed to 10^{-1}. The divergence decreases following a power law: $\mathrm{Div}(\boldsymbol{V}) = aN^{-b}$; the parameters a and b are given in Table 2.

For a same grid, the divergence is smaller when the slip length is larger: the small length scales introduced by the slip model require more modes to be accounted for. When compared to the case of the polynomial filter, the divergence behavior is quite similar. Only the power differs, the decrease being greater ($b = 4$) with a polynomial regularization. This is not very surprising because the physical approach introduces new partial derivatives on all boundaries; their impact on the mathematical properties of the solution are unknown. This more important complexity of the physics in the case of slip conditions can also be observed on the way global quantities converge following the used slip length. In Fig. 13 are presented, with respect to the number of Chebyshev modes, the relative difference (in L_2 norm)

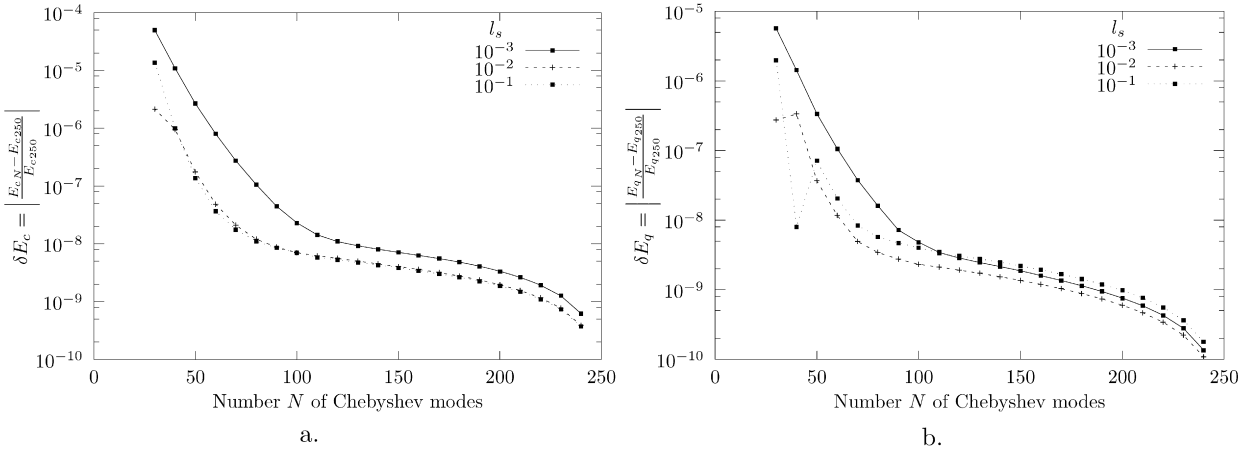

Fig. 13. Convergence of the relative kinetic energy (a) and of the relative thermal energy (b), for $Vi = 10^{-1}$, $l_s = 10^{-3}$, 10^{-2} and 10^{-1}.

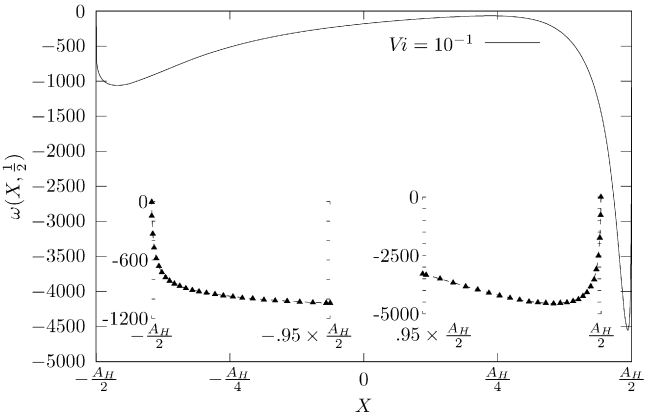

Fig. 14. Vorticity profile on the free surface at $Ma = 1500$, $Pr = 1$, $Vi = 10^{-1}$ and $l_s = 10^{-3}$.

between the kinetic (left panel) and thermal (right panel) energies and their values obtained with the finest mesh (namely 250×250). All the curves decrease, first rapidly up to $N \in [50, 100]$, then more slowly.

The flow fields are quite similar to those calculated with interface viscosity alone. Nevertheless, the extrema are modified. For $l_s = 10^{-3}$, the vorticity maximum (not shown, located on the solid boundaries) is of $\sim 30\%$ less, going from 5000 to 3500, while the minimum slightly varies from -4900 to -4500 (see Fig. 14). This is directly related to the scale of the thermal gradient in the cold corner. The slip conditions applying on the solid boundaries, their impact on the scales on the free surface is not direct. On the contrary, since the positive vorticity values come from the viscous dissipation on the solid walls, the slip reduces the stress and subsequently the maximum of vorticity, even for as small a value as $l_s = 10^{-3}$. The vorticity profile along the free surface, shown in Fig. 14, exhibits the impact of the slip conditions. As in the case of interface viscosity alone (see Fig. 10(b)), the curve presents two minima but now the vorticity continuously cancels in the corners contrary to what was observed without slip conditions. Nevertheless the vorticity gradients at the solid/fluid junctions are important.

The velocity profiles along the boundaries are displayed in Fig. 15. On the bottom wall (right upper panel), the negative horizontal velocity is linked to the primary vortex while the positive values exhibit secondary vortices in the bottom corners. $\frac{\partial u}{\partial x}$ (upper left panel) does not cancel in the corners which, coupled to the continuity constrain, leads to the sharp gradients of the vertical velocity in the warm and cold corners which can be observed in the left and right low panels respectively.

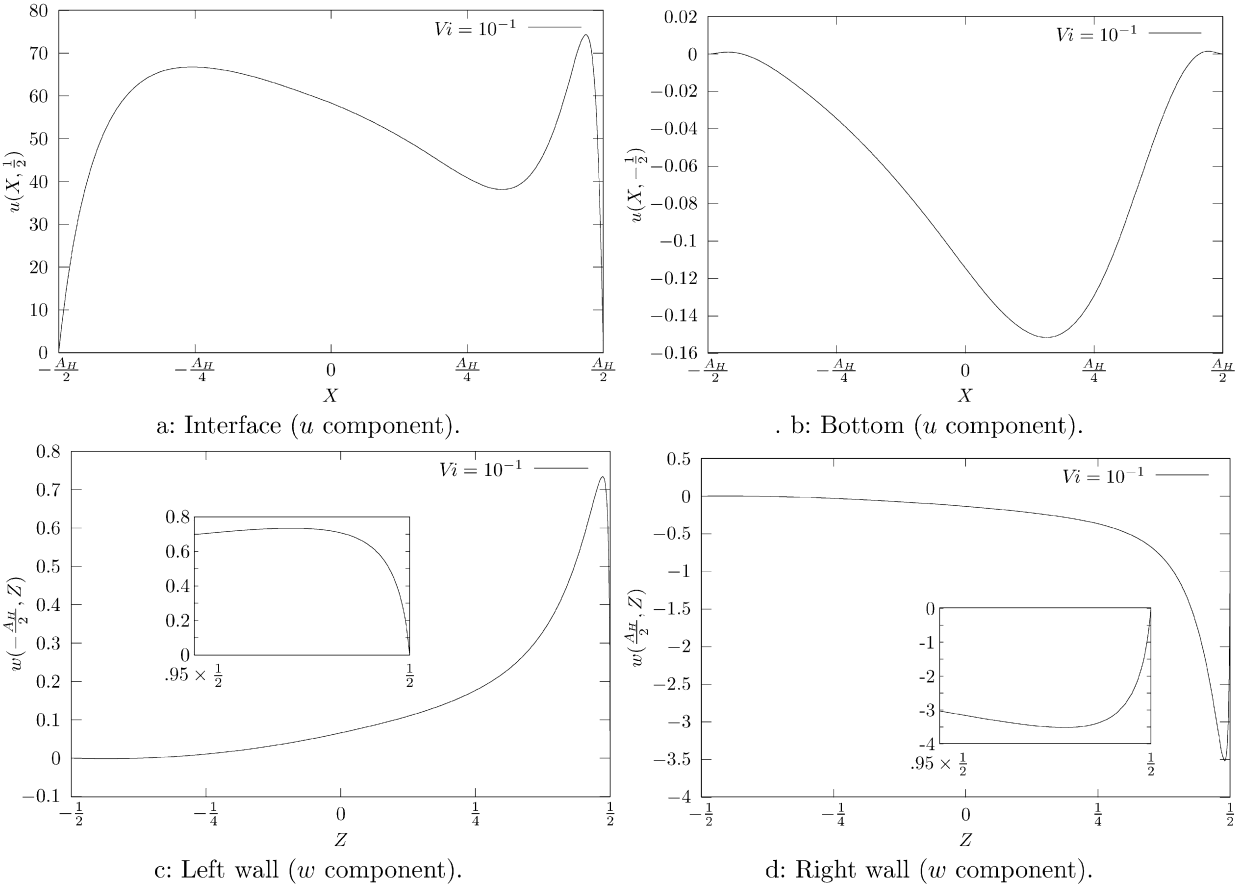

a: Interface (u component). . b: Bottom (u component).

c: Left wall (w component). d: Right wall (w component).

Fig. 15. Velocity profiles along the boundaries ($Ma = 1500$, $Pr = 1$, $Vi = 10^{-1}$ and $l_s = 10^{-3}$).

The model is however regular and provides a finite value of the pressure maxima based on physical fluid properties. Let us note that, with the chosen values of Vi and l_s, the obtained solution is closer to the $n = 80$ reference solution than to the low order $n = 4$ filtered results, as illustrated by Figs. 5, 7, 14 and 15(a).

4. Conclusions

The vorticity singularity of wall confined thermocapillary flows remains for any realistic imposed angle, even with the use of a slip boundary condition. It was shown that the incompressibility condition is not enforced when interface viscosity is used alone. Both conditions, interface viscosity and slip, have to be used to let the divergence cancel at the junctions. All the models should converge towards the singular model when increasing the regularization parameter or when decreasing the slip length and the interface viscosity values.

None of the methods used in order to remove the vorticity singularity allow the exponential decrease of the velocity divergence with the mesh refinement, as expected for a regular solution. A polynomial decreasing law is observed for the model coupling interfacial viscosity with slip boundary conditions as well as for a polynomial filter. The decrease is faster with the polynomial filter, but leads to infinite pressure values when decreasing the filtering length. The use of interface viscosity and slip introduces physical scales which limit the divergence of the pressure. These scales are physically relevant since they could be experimentally determined.

Spectral methods revealed to be well adapted to this type of analysis which necessitates a fine resolution of the small scales they introduce. Their main advantage is to highlight the presence of the singularities of the models.

If the interest of accounting for such phenomena as interfacial viscosity or slip can be questioned for large systems (meters), they can become predominant for the design of small scale devices.

This study is based on the a-priori hypothesis of incompressible Newtonian fluid flows. It gives some indications on the compatibility of some boundary conditions, based on microscopic considerations, with a macroscopic description of the flows. It does not give a final point to the question of which model should be used: this would necessitate collecting precise measurements of interface viscosity and slip length scale values, coupled with precise experiments in small devices.

Acknowledgements

The authors wish to thank the referees for their help in improving the quality of the manuscript.

The simulations were performed at Université Paris XI Orsay on the computers of the Centre de Ressources Informatiques. Figs. 2 and 11 were created with JPicEdt and Figs. 3, 5, 7, 8, 9, 10, 12, 13, 14 and 15 were obtained by modifying Gnuplot pstricks outputs with JPicEdt. JPicEdt is developed under the GPL License.

References

[1] H.K. Moffatt, Viscous and resistive eddies near a sharp corner, J. Fluid Mech. 18 (1964) 1–18.
[2] D. Canright, Thermocapillary flow near a cold wall, Phys. Fluids 6 (4) (1994) 1415–1424.
[3] H.C. Kuhlmann, Thermocapillary Convection in Models of Crystal Growth, first ed., Springer Tracts in Modern Physics, vol. 1, Springer, 1999.
[4] E.B. Dussan, On the spreading of liquids on solid surfaces: static and dynamic contact lines, Annu. Rev. Fluid Mech. 11 (1979) 371–400.
[5] L.M. Pismen, Mesoscopic hydrodynamics of contact line motion, Colloids and Surfaces A 206 (2002) 11–30.
[6] G. Kasperski, G. Labrosse, On the numerical treatment of viscous singularities in wall-confined thermocapillary convection, Phys. Fluids 12 (11) (2000) 2695–2697.
[7] É. Chénier, C. Delcarte, G. Kasperski, G. Labrosse, Sensitivity of the liquid bridge hydrodynamics to local capillary contributions, Phys. Fluids 14 (2002) 3109–3117.
[8] S. Nguyen, C. Delcarte, G. Kasperski, G. Labrosse, Singular boundary conditions and numerical simulations: lid-driven and thermocapillary flows, in: R. Savino (Ed.), Surface Tension Driven Flows and Applications, Research Signpost, 2006, pp. 121–146 (Chapter 5).
[9] W.W. Schultz, N.-Y. Lee, J.P. Boyd, Chebyshev pseudospectral method of viscous flows with corner singularities, J. Sci. Comput. 4 (1989) 1–24.
[10] O. Botella, R. Peyret, Computing singular solutions of the Navier–Stokes equations with the Chebyshev-collocation method, Int. J. Numer. Methods Fluids 36 (2) (2001) 125–163.
[11] F. Auteri, N. Parolini, L. Quartapelle, Numerical investigation on the stability of singular driven cavity flow, J. Comput Phys. 185 (2002) 1–25.
[12] A. Zebib, G.H. Homsy, E. Meiburg, High Marangoni number convection in a square cavity, Phys. Fluids 28 (12) (1985) 3467–3476.
[13] M.J. Boussinesq, Sur l'existence d'une viscosit superficielle dans la mince couche de transition sparant un liquide d'un autre fluide contigu, Ann. Chim. Phys. 29 (1913) 349–364.
[14] L.E. Scriven, Dynamics of a fluid interface. Equation of motion for Newtonian surface fluids, Chem. Eng. Sci. 12 (1960) 98–108.
[15] S. Goldstein, Note on the conditions at the surface of contact of a fluid with a solid, in: The Oxford Engineering Science Series, vol. 2, Clarendon Press, Oxford, 1938, pp. 676–680.
[16] S. Nguyen, C. Delcarte, A spectral collocation method to solve Helmholtz problems with boundary conditions involving mixed tangential and normal derivatives, J. Comput. Phys. 200 (2004) 34–49.
[17] V.C. Regnier, P.M. Parmentier, G. Lebon, J.K. Platten, Numerical simulations of interface viscosity effects on thermoconvective motion in two-dimensional rectangular boxes, Int. J. Heat Mass Transfer 38 (14) (1995) 2539–2548.
[18] M.A. Vila, V.A. Kuz, A.E. Rodríguez, Surface viscosity of pure liquids, J. Colloid Interface Sci. 107 (2) (1985) 314–321.
[19] D. Bedeaux, I. Oppenheim, Hydrodynamic response and free surface modes for two immiscible fluids, Physica A 90 (1978) 39–57.
[20] F.C. Goodrich, Theory of capillary excess viscosity, Proc. R. Soc. London Ser. A 374 (1981) 341–367.
[21] C. Canuto, M. Hussaini, A. Quarteroni, T. Zang, Spectral Methods in Fluid Dynamics, Springer-Verlag, New York, 1988.
[22] A. Batoul, H. Khallouf, G. Labrosse, Une méthode de résolution directe (pseudo-spectrale) du problème de Stokes 2d/3d instationnaire. application à la cavité entrainée carrée, C. R. Acad. Sci. Paris 319 (I) (1994) 1455–1461.
[23] E. Leriche, G. Labrosse, High-order direct Stokes solvers with or without temporal splitting: numerical investigations of their comparative properties, SIAM J. Sci. Comput. 22 (4) (2000) 1386–1410.
[24] D.H. Haidvogel, T.A. Zang, The accurate solution of Poisson's equation by expansion in Chebyshev polynomials, J. Comput. Phys. 30 (1979) 167–180.
[25] Private communication with X.
[26] S. Nguyen, Dynamique d'une interface en présence d'une singularité de contact solide/fluide, Ph.D. thesis, Université Paris XI, Orsay, 2005.